China Geology 8 (2025) 765−778

China Geology

Journal homepage: http://chinageology.cgs.cn
https://www.sciencedirect.com/journal/china-geology

Investigation on the fracture propagation for horizontal wells in hydrate reservoirs using a fluid-solid coupling discrete element method

Jia-wei Zhang[a, b], Chang-ling Liu[b, c,*], Yong-chao Zhang[b, c,*], Le-le Liu[b, c], Yun-kai Ji[b, c]

[a] *Chinese Academy of Geological Sciences*, *Beijing* 100037, *China*
[b] *Key Laboratory of Gas Hydrate of Ministry of Natural Resources*, *Qingdao Institute of Marine Geology*, *Qingdao* 266237, *China*
[c] *Laboratory for Marine Mineral Resources*, *Qingdao Marine Science and Technology Center*, *Qingdao* 266237, *China*

ARTICLE INFO

Article history:
Received 4 March 2024
Received in revised form 11 July 2024
Accepted 18 September 2024
Available online 10 October 2024

Keywords:
Hydraulic fracturing technology
Gas hydrate reservoirs
Hydrate-bearing sediment
Discrete element method
Fluid-solid coupling
Hydraulic fracturing
Horizontal wells
Fracture propagation
Oil-gas exploration engineering

ABSTRACT

Hydraulic fracturing technology has played an important role in the exploitation of unconventional oil and gas resources, however, its application to gas hydrate reservoirs has been rarely studied. Currently, there is still limited understanding of the propagation and extension of fractures around the wellbore during the fracturing process of horizontal wells in hydrate reservoirs, as well as the stress interference patterns between fractures. This study simulates hydraulic fracturing processes in hydrate reservoirs using a fluid-solid coupling discrete element method (DEM), and analyzes the impacts of hydrate saturation and geological and engineering factors on fracture extension and stress disturbance. The results show that hydraulic fracturing is more effective when hydrate saturation exceeds 30% and that fracture pressure increases with saturation. The increase in horizontal stress differential enhances the directionality of fracture propagation and reduces stress disturbance. The distribution uniformity index (DUI) reveals that injection pressure is directly proportional to the number of main fractures and inversely proportional to fracturing time, with fracturing efficiency depending on the spacing between injection points and the distance between wells. This work may provide reference for the commercial exploitation of natural gas hydrates.

1. Introduction

Natural gas hydrates are recognized as a promising source of clean energy with the potential to replace conventional oil and gas resources in the 21st century. Abundant hydrate deposits have been found in continental shelf sediments and continental permafrost regions (Sun CY et al., 2011). The estimated reserves of natural gas in hydrates are about twice the amount of conventional fossil energy resources (Ruppel CD and Kessler JD 2017; Shaibu R et al., 2021; Su PB et al., 2024). In the Shenhu area of the South China Sea, China has conducted two consecutive hydrate production trials, the second of which employed horizontal well fracturing technology (Li JF et al., 2018; Ye JL et al., 2020). Despite advancements in both daily and cumulative gas production, achieving commercial production remains a challenge (Chen XJ et al., 2022; Chen MT et al., 2023a). Therefore, enhancing horizontal well fracturing is essential for achieving commercial production of hydrate resources (Wu P et al., 2020; Xu JC et al., 2023; Li XY et al., 2024b).

Both horizontal well fracturing and simultaneous hydraulic fracturing in multiple horizontal wells have been adopted in the field of unconventional oil and gas development (Lei Q et al., 2022; Zhao JZ et al., 2018). Horizontal well fracturing increases the effective contact area between the wellbore and the reservoir compared to traditional vertical well fracturing (Liao SZ et al., 2022). Simultaneous hydraulic fracturing in multiple horizontal wells further enhances the complexity of the induced fracture network, leading to improved operational efficiency and cost reduction. In contrast, hydrate reservoirs are typically characterized by weak cementation and lack of consolidation among sedimentary particles, and low permeability (Li YH et al., 2021; Zhang Z et al., 2023; Dong L et al., 2024; Zhang YC et al., 2022). However, the hydrate in sedimentary pores

First author: *E-mail address*: zhangjwsw@qq.com (Jia-wei Zhang).

* Corresponding author: *E-mail address*: qdliuchangling@163.com (Chang-ling Liu); yongchao.zhang@hotmail.com (Yong-chao Zhang).

Literary editor: Xi-jie Chen
doi:10.31035/cg2024031
2096-5192/© 2025 China Geology Editorial Office.

strengthens the cementation among these particles, rendering the mechanical properties of hydrate-bearing sediments (HBS) being similar to those of consolidated rocks (Jung JW and Santamarina JC 2011). Research has shown that hydrate reservoirs can be effectively fractured, offering the potential for enhancing the extraction efficiency of gas hydrates. (Feng YC et al., 2019; Sun JX et al., 2019; Wang ZY et al., 2018). Too JL et al. (2018) carried out three-point bending experiments on HBS with different hydrate saturations and found that HBS with high hydrate saturation exhibited similar fracture toughness to sandstone samples. Konno Y et al. (2016) conducted fracturing experiments on HBS and observed that the fracturing damage pattern of HBS also showed similarities with sandstones. The permeability of the samples still increased to some extent after fracture closure compared to before fracturing. Subsequent studies (Ma KL et al., 2023; Li B et al., 2024a) further indicated that HBS becomes more brittle with increasing hydrate saturation, and the use of high-viscosity fracturing fluids would increase the number of fractures produced. Using an analytic hierarchy process-entropy method, Liu XQ et al. (2020) found that the feasibility of fracturing on HBS can be evaluated using a feasibility index determined by hydrate saturation, mineral composition and stress anisotropy. Although research based on physical experiments has made some progress, these methods are limited by factors such as the difficulty of sample preparation and high costs, making it challenging to achieve a deep understanding of the fracturing mechanisms in hydrate reservoirs (Li FG et al., 2019). Commonly used numerical simulation methods for hydraulic fracturing in oil and gas reservoirs include Finite element method (FEM), Finite Difference Method (FDM) and Discrete element method (DEM) (Chen MT et al., 2023b). Liu Y et al. (2023) used hydraulic fracturing-assisted depressurization development to simulate hydraulic fracturing of hydrate reservoirs in the South China Sea and found that hydraulic fracturing can significantly increase gas production in low-permeability reservoirs. Using the FEM, Chen C et al. (2000) demonstrated that hydraulic fracturing increases the hydrate decomposition rate by four times compared to single-well depressurization. However, this method cannot to capture inter-fracture interactions and reservoir non-homogeneity caused by hydrate distribution, which is a significant limitation (Deng SC et al., 2014). DEM is more appropriate as it accurately represents the mechanical response of the material and accurately captures the initiation, propagation, and final pattern of fractures (Ishida MT 2011; Ding YL et al., 2022). Yao YX et al. (2021) found that hydrate reservoirs with higher hydrate saturation were able to produce effective main fractures after hydraulic fracturing. Liu H et al. (2023) embedded a discrete fracture model in Tough+Hydrate to simulate hydraulic fracturing in clay hydrate reservoirs and found that hydraulic fracturing, led to a significant increase of approximately 300% in methane production. Yu T et al. (2021) established a horizontal well fracturing model for low-permeability multilayer hydrate reservoirs using test-mining field data from the Shenhu Sea area in the South China Sea and found that the horizontal fracture could greatly promote the long-term production of natural gas from the reservoir. The stress distribution and fracture network within reservoirs become more intricate when multiple horizontal wells undergo simultaneous fracturing. However, current research on these issues remains inadequate.

This study employs coupled fluid-solid DEM to investigate fracture propagation patterns and stress disturbances between fractures during the simultaneous fracturing of horizontal wells in hydrate reservoirs. The influence of various factor on the fracturing efficacy was quantitatively assessed using the fracture distribution uniformity index. The results are expected to provide valuable insights for well pattern deployment and fracturing parameter in hydrate reservoirs.

2. Numerical model

A DEM is used to simulate the movement, deformation, and interaction of particles to characterize and analyze the overall mechanical behavior of a material. With this method, micromechanical parameters (such as bond strength and friction coefficient) play a pivotal role in determining the model's accuracy. To enhance the model's applicability and precision, calibration using experimental data is essential. In this study, the micromechanical parameters of the numerical model are calibrated with physical experiments to accurately reproduce the model's mechanical properties. Furthermore, a hydraulic fracturing model for hydrate reservoirs was established, employing micromechanical parameters calibrated using triaxial compression experimental data. The calibrated fluid parameters ensure the validity and accuracy of the fracturing simulation.

2.1. Discrete element method for fluid-solid coupling

Force and displacement are shown in the DEM through a bonding model between particles (Tavarez FA and Plesha ME 2007). Different materials require the selection of appropriate bonding models based on their constitutive models. In this study, the mechanical model of HBS was simulated using the parallel bonding model. The model consists of a collection of springs with tangential and normal stiffness, generating forces and moments within the bond as particles move relative to each other. When the forces and moments exceed the bond strength, bond failure occurs (Eq. 1). Subsequently, these forces and moments are removed from the bond, resulting in fracturing (Fig. 1a):

$$\bar{\sigma} = \frac{\bar{F}_N}{\bar{A}} + \bar{\beta}\frac{\left\|\bar{M}_b\right\|\bar{R}}{\bar{I}}$$
$$\bar{\tau} = \frac{\bar{F}_s}{\bar{A}} \quad (1)$$

Where $\bar{\sigma}$ is the parallel bond strength, MPa; $\bar{F}_N$ is the normal force, MPa; $\bar{F}_s$ is the tangential force，MPa; $\bar{M}_b$ is the bending moment, kN/m; $\bar{R}$ is the average radius of the two

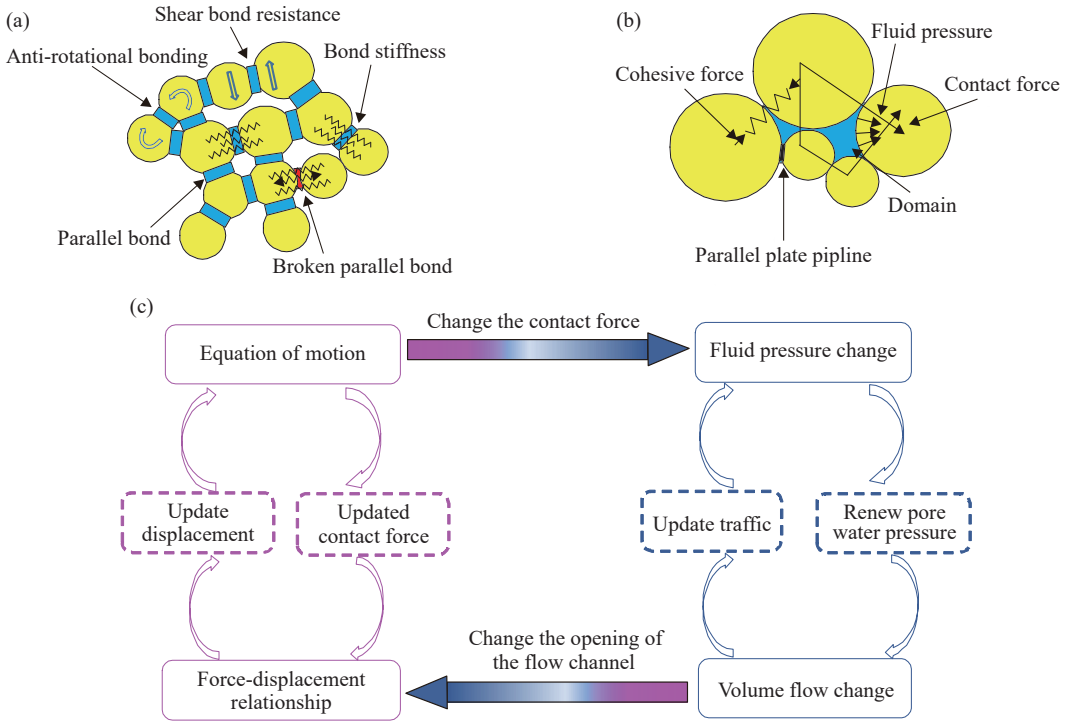

Fig. 1. Schematic diagram of DEM fluid-coupling model. a–parallel bonding model. b–fluid-solid coupling element model. c–calculation procedure of hydro-mechanical model (modified from Zhou J et al., 2016).

contacting particles, m; $\bar{A}$is the cross sectional area of the particles, m^2; $\bar{I}$ is the moment of inertia, m^4; and $\bar{\beta}$ is the moment contribution factor.

Fig. 1b illustrates the fluid-solid coupling schematic in the DEM model, which comprises two main components: parallel plate pipeline and domain (Zhou J et al., 2016). The yellow color represents material particles, the blue areas enclosed by particles represent the domains, and the black short lines denote particle contacts. The fluid-solid coupling model based on DEM involves two critical concepts: flow channels and domains. In this model, the contacts between particles are treated as pairs of parallel plates with an initial aperture. These contacts not only transmit loads but also serve as flow channels for fracturing fluid. The domain refers to the pore space formed by several adjacent particles. These domains are interconnected by flow channels, forming a complete fluid flow network.

Fig. 1c presents the computational logic of fluid-solid coupling in the DEM model. With the injection of fluid, the pressure difference between adjacent domains changes due to factors such as fracturing fluid volume changes and particle movements, driving the fluid transfer through the flow channels. The net fluid flow variation in the domains induces changes in the local pore pressure. This variation in pore pressure further influences the movement of particles surrounding the domains, leading to changes in the volume of the domains and the apertures of the flow channels. During the hydraulic fracturing process, the flow of fracturing fluid and the movement of particles interact, jointly participating in the fluid-solid coupling computation.

In the coupled fluid-solid model, the fluid within the parallel plates is presumed to exhibit laminar flow characteristics. The volumetric flow rate of the fluid flowing through the interstitial channels between particles adheres q_i to Eq. 2:

$$q_i = \frac{\omega^3}{12\mu_v}\frac{\Delta p_i}{l_i} \tag{2}$$

where ω is the initial runner opening, m; Δp_i is the pressure difference between the two domains, MPa; μ_v is the fluid viscosity coefficient, Pa.s; l_i is pipe length, m.

The model undergoes iterative calculations to update the pore pressure within the storage area. The pressure differential Δp_f P of pore water in the same storage area can be expressed as:

$$\Delta p_f = \frac{K_f}{V_d}\left(\sum q_i \Delta t - \Delta V_d\right) \tag{3}$$

where K_f is fluid bulk modulus, pa.s; V_d is volume of water between particles, m^3; Δt is Fluid injection time, s.

During the solution process, it is imperative that the change in inlet pressure remains below the perturbation pressure. The critical time step Δt is defined as follows:

$$\Delta t = \frac{24 u_v \bar{R} V_d}{N K_f \omega^3} \tag{4}$$

2.2. Numerical model establishment and validation

To ensure that the numerical model for hydraulic fracturing in hydrate reservoirs accurately reflects the mechanical properties of actual reservoirs, this study

calibrates the micromechanical parameters by comparing the triaxial compression numerical model with physical experimental data. The physical experimental data were obtained from our team previous undrained triaxial shear experiments conducted on fine-grained sediments in the Shenhu area of the South China Sea (Wei RC et al., 2023).

The samples are fine-grained sediments from the Shenhu area of the South China Sea. The experimental data include stress-strain relationships of sediments with 30% and 50% hydrate saturations under a pressure of 2 MPa. Using the parallel bonding model described in Section 2.1, a standard specimen without hydrate was generated with a diameter of 38 mm and a height of 76 mm. To maintain consistency with the consolidation degree of the physical experimental samples, *in-situ* stresses were applied post-model generation to ensure particle contact. The hydrate particles were then randomly generated in the pores between the sediment particles according to the preset hydrate saturation (Eq. 5) and dispersed through full contact movement between the sediment particles and hydrate particles (Fig. 2a). Modeling results show that hydrates exist in sediment pores in three configurations: Cemented, load-bearing granular, and cement pore-filling. This approach aligns with the research conducted by Yao YX et al (2021). Numerical models with 30% and 50% hydrate saturations were established, with the micromechanical parameters between particles iteratively adjusted to accurately reflect the models' micromechanical properties. First, the mechanical parameters of the triaxial shear numerical model were calibrated with the experimental results of samples with 30% hydrate saturation. The parameters including parallel bond normal strength, internal friction angle and stiffness ratio were adjusted to align the simulation outcomes with the experimental data. Subsequently, the calibrated model was verified using experimental results from samples with 50% hydrate saturation. If significant discrepancies were observed between the numerical simulation and the experimental results, further adjustments were made to the parameters derived from the 30% saturation model until the stress-strain curves from both the simulation and experimental results were in good agreement. To minimize boundary effects on simulation results, the model boundary was constrained by filling the medium with small particles to maintain the required confining pressure (Li ZF et al., 2022). The confining pressure was set at 2 MPa, and the loading rate was 0.04%/min to ensure quasi-static loading of the model.

$$S_h = \frac{nP_s}{V_S S_s} \tag{5}$$

where S_h is sample hydrate saturation, %; n is number of hydrate particles; P_s is individual hydrate particle area; V_s is sediment porosity; S_s is total sample area, m^2.

Table 1 shows the results of the calibrated numerical model micromechanical parameters, compared with physical experimental data under different hydrate saturation conditions. The numerical simulation results (Fig. 2b) reveal that the stress-strain curve trends from physical experiments and simulations conducted under different saturation conditions are largely in agreement. The peak strength of the samples increases with higher hydrate saturation. This increase is attributed to the dual role of hydrates in both cementation and increasing the overall sediment density (Hyodo M et al., 2017). The failure mode of the sample is shear failure. Before reaching the peak deviator stress, the model shows a high degree of agreement with the physical experimental results, indicating a better correlation. Consequently, the micromechanical parameters of the model are considered accurate at this stage (Gu XQ et al., 2014).

The micromechanical parameters calibrated by the triaxial shear numerical model are used to establish a hydraulic fracturing model for a single-well hydrate reservoir (Fig. 3a). The model is a square of 50 m side length has a closed boundary. To ensure effective hydraulic fracturing, the model was validated by comparison with the established model of Yao YX et al. (2021). Hydrate saturation was maintained at 50% in accordance with the cited literature, and the maximum and minimum horizontal stresses (σ_{Hmax} and σ_{Hmin}) were set at 4 MPa and 2 MPa, respectively.

The injection point was located at the center of the reservoir, and the injection pressure was set at 10 MPa and held constant until the reservoir fractured. Fig. 3b shows the simulation results of the fracturing behavior validation model.

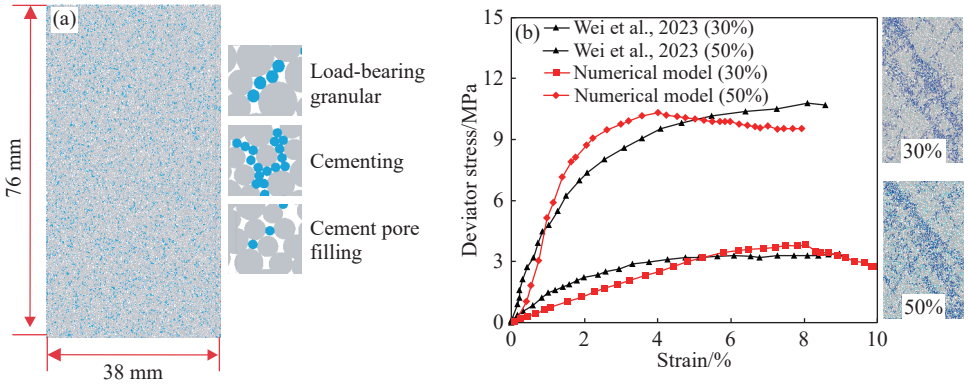

Fig. 2. Numerical model calibration results. a–triaxial shear numerical model for HBSs. b–numerical model and experimental stress-strain curve with different saturation.

Table 1. Micromechanical parameters of the numerical model.

Micro-parameters	Deposit Sediment	Hydrate	Hydrate and deposit Sediment cement
Minimum particle size/m	0.1	0.06	\
Maximum to minimum particle size ratio	1.66	1	\
Density/Kg.m^{-3}	2730	900	\
friction coefficient	0.5	0.8	0.8
Parallel bond normal strength/MPa	6	10	10
Parallel bond shear strength/MPa	7	10.5	10.5
Internal friction angle/°	30	35	35
Stiffness ratio	0.8	1.2	1.2

It can be seen that with the number of fractures remaining constant, the well pressure increases linearly until new fractures are formed. Especially, fracture propagate vertically in bi-wing fracture form along the maximum horizontal principal stress direction. The fracture pattern is not symmetrical and bifurcates with increasing extension distance. The simulation results demonstrate the fracture initiation and propagation processes are consistent with fracture mechanics theory and the experimental results of Zhou J et al. (2010).

2.3. Simulation scheme

During hydraulic fracturing, fracture initiation and propagation are influenced by both geological and engineering factors. Based on the research by Liu XQ et al. (2020) research on the fracture ability of hydrate reservoirs and the direction of well network optimization in actual fracturing processes, this study identified five factors that significantly affect fracturing: Hydrate saturation, horizontal stress differential, injection pressure, injection point spacing, and horizontal well spacing. A model was constructed for the simultaneous fracturing of two horizontal wells in a 50 m × 50 m square hydrate reservoir, as shown in Fig. 4. In the models with different saturation levels, the specific number of particles is as follows: The model with 20% hydrate saturation contains 21026 particles; the model with 30% hydrate saturation contains 23056 particles; the model with 50% hydrate saturation contains 27812 particles; and the model with 70% hydrate saturation contains 32904 particles. Each horizontal well was set up with four injection points, where d is the injection point spacing and h is the spacing between the two horizontal wells. The orthogonal experimental method was used for the experimental design, and the simulation scheme is detailed in Table 2. The baseline model, numbered 0-0, has micromechanical and fluid parameters that are the same as the fracture behavior validation model described in section 2.2. During the simulation, only the factors to be studied were changed, while the other micromechanical and fluid parameters of the model remained consistent with the baseline model (0-0).

3. Simulation results

3.1. Influence of different hydrate saturations on fracture propagation

Fig. 5 shows the fracture distribution in hydrate reservoirs with different hydrate saturations post-fracturing. In hydrate reservoirs with 10% hydrate saturation, the poorly consolidated area around the perforation points is rapidly invaded by fluid after fracturing, leading to hydrate reservoir damage and the creation of numerous fractures. When hydrate saturation exceeds 30%, the reservoir develops main fractures in different directions. Due to the in-situ stresses, these fractures do not interconnect to form a fracture network. As hydrate saturation increases, the cementation strength between sediment particles significantly increases, necessitating higher fluid pressures within fractures to induce reservoir rupture. Moreover, the different mechanical properties of hydrate and sediment lead to fracture bifurcation and deviation.

Fig. 6 shows the breakdown pressure and fracture propagation trends in reservoirs with different hydrate

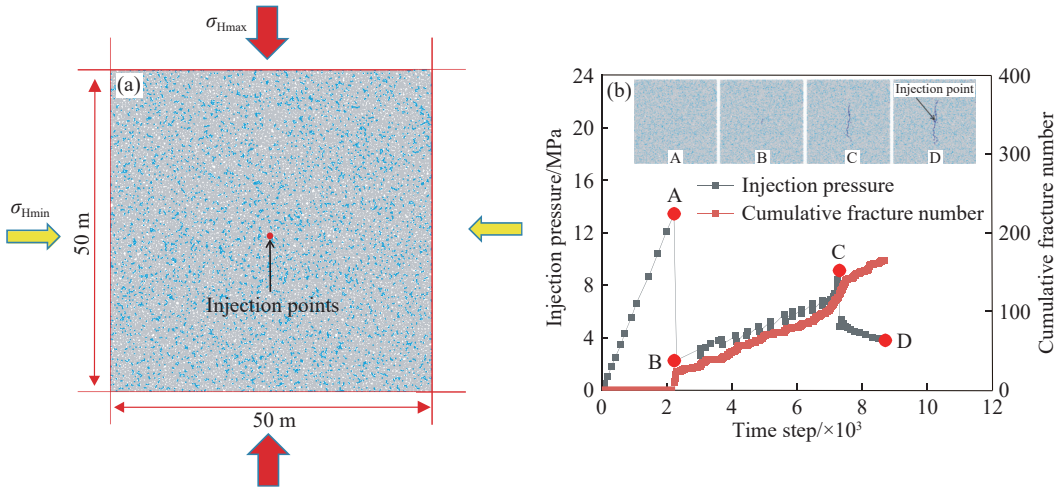

Fig. 3. Hydraulic fracturing model and fracturing calibration of hydrate reservoir. a–fracture behavior validation model. b–hydraulic fracturing model validation results.

saturation. The cumulative number of fracture refers to the total number of fractures formed in the HBSs when the bonds between sedimentary particles and hydrate particles are destroyed by bonding forces under the action of fluid pressure. The number of hydrate fractures specifically refers to the fractures formed between hydrate particles due to the failure of bonding forces under fluid pressure. The curves show that the increase in reservoir breakdown pressure increases as hydrate saturation increases (Fig. 6a). Additionally, the number of fractures within the hydrate area increases after fracturing as hydrate saturation increases. Therefore, hydraulic fracturing can effectively alter the occurrence state of hydrate as saturation increases. The radius of fracture extension post-fracturing represents the scale of hydraulic fracturing to some extent (red circles in Fig. 5a). When hydrate saturation is below 50%, the average fracture extension radius increases with increasing hydrate saturation. When the hydrate saturation is higher than 50%, the average fracture extension radius remains relatively unchanged, indicating that fracture formation and propagation are affected to different degrees at different hydrate saturation levels (Fig. 6b).

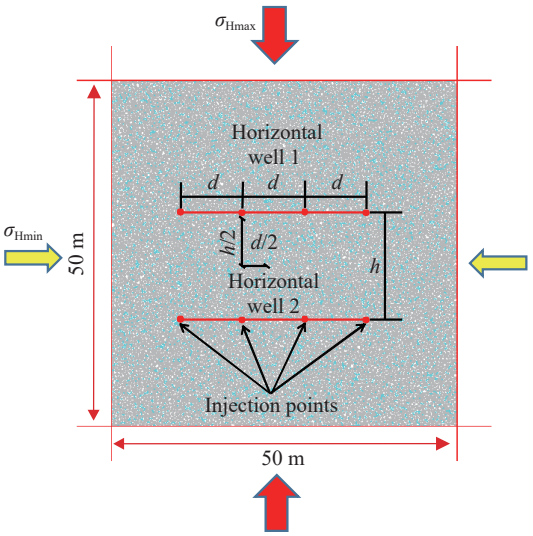

Fig. 4. Modeling of horizontal well fracturing in hydrate reservoirs.

3.2. Effect of different horizontal stress differences on fracture propagation

The distribution of fractures in hydrate reservoirs under different horizontal stress differentials is shown in Fig. 7 When the horizontal stress difference is 0 MPa, multiple main fractures are formed around the injection points, particularly diverging between the two injection points. In this scenario, the formation of fractures is significantly influenced by the

Table 2. Fracturing simulation scenarios with different influencing factors.

Model number	Hydrate saturation/ %	Horizontal stress difference/ MPa	Injection pressure/ MPa	Injection point spacing/ m	Horizontal well spacing/ m
0–0	50	2	10	10	16
1–1	10	2	10	10	16
1–2	30				
1–3	50				
1–4	70				
2–1	50	0	10	10	16
2–2		2			
2–3		4			
2–4		6			
3–1	50	2	5	10	16
3–2			10		
3–3			15		
3–4			20		
4–1	50	2	10	10	8
4–2					12
4–3					16
4–4					20
5–1	50	2	10	6	16
5–2				10	
5–3				14	
5–4				18	

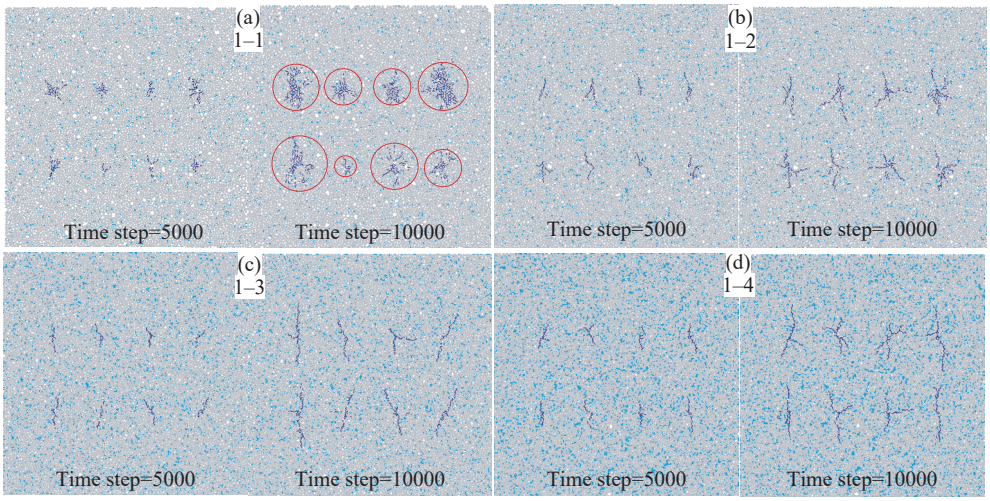

Fig. 5. Fracture distribution after reservoir fracturing under different hydrate saturation. a–hydrate saturation 10%. b–hydrate saturation 30%. c–hydrate saturation 50%. d–hydrate saturation 70%.

distance between adjacent injection points, resulting in a multi-fracture damage pattern. At a horizontal stress difference of 2 MPa, fractures predominantly propagate in the direction of the maximum horizontal principal stress, resulting in multiple branching cracks near the injection points. Increasing the differential horizontal stress reduces the number of branch fracture around the injection point, causing the fractures to primarily extend in the direction of the maximum horizontal principal stress. An increase in the horizontal stress differential is noted to reduce the impact of injection point spacing on fracture propagation. When the fracture tips of two horizontal wells approach each other, bifurcation and deviation of the tips occur, indicating an enhanced influence of horizontal well spacing on fracture propagation.

Fig. 8 shows the relationship between the number of fractures, time steps, fracture pressure, and fracture extension radius under different horizontal stress differentials. Increasing the horizontal stress differential shortens the time required for reservoir rupture and reduces the cumulative number of fractures. Under conditions of low horizontal stress differential, multiple shorter main fractures predominate; however, with higher stress differences, bi-wing fractures with longer extension radii are generated. The breakdown pressure of the reservoir decreases as the horizontal stress difference increases.

3.3. Effect of fluid injection pressure on fracture propagation

Fig. 9 shows that at an injection pressure of 5 MPa, only a few fractures are initiated at certain injection points by the 500th time step. As the time step progresses, gradual damage and the formation of short fractures occur around the injection point. During this phase, the fracturing fluid mainly infiltrates, causing limited damage to the hydrate reservoir. At an injection pressure of 10 MPa, the post-fracturing fracture network is more complex than at 5 MPa, characterized mainly by bi-wing fractures parallel to the maximum horizontal principal stress direction with some branching fractures. As the injection pressure is further increased, multiple main fractures develop around the injection points, and microcracks emerge due to stress perturbations. When an injection pressure of 20 MPa is reached, several main fractures and a significant number of branching fractures appear around the

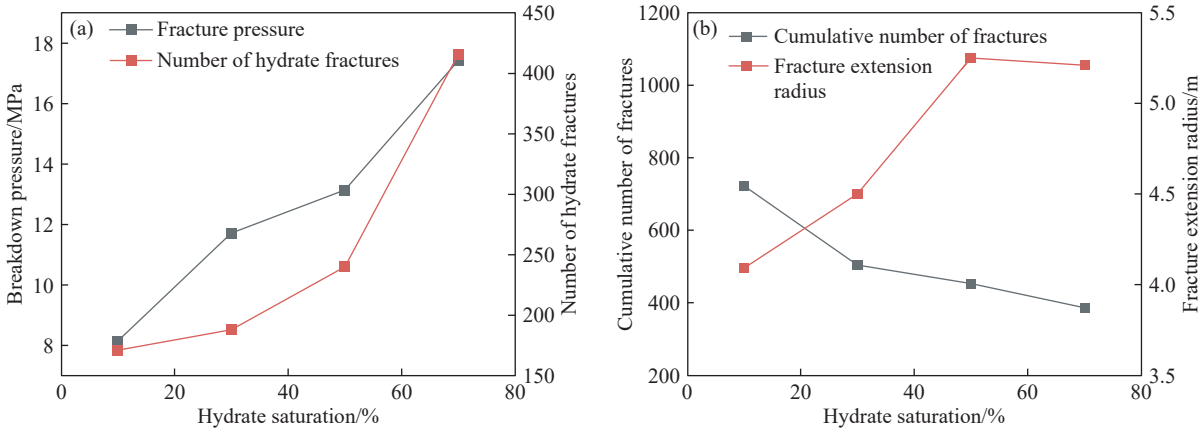

Fig. 6. Breakdown pressure and fracture propagation trends in reservoirs with different hydrate saturation. a–breakdown pressure and number of hydrate fractures. b–cumulative number of fracture and extension radius.

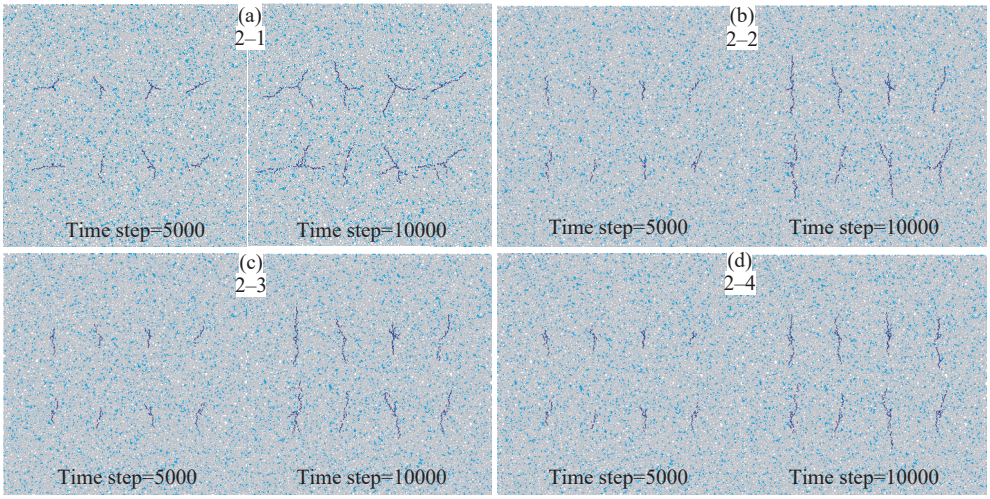

Fig. 7. Fracture distribution after reservoir fracturing under different horizontal stress differential. a–horizontal stress differential of 0 MPa. b–horizontal stress differential of 2 MPa. c–horizontal stress differential of 4 MPa. d–horizontal stress differential of 6 MPa.

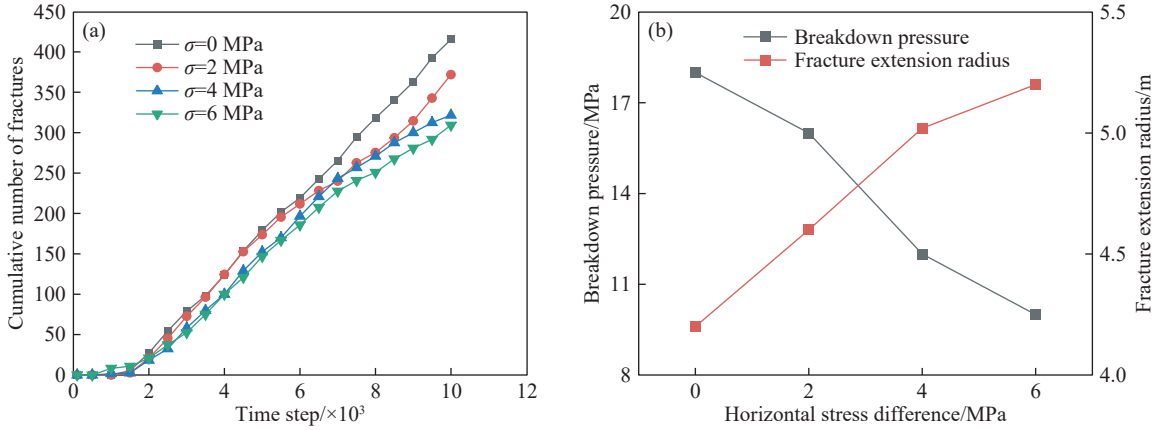

Fig. 8. Reservoir fracture pressure and fracture propagation trends under different horizontal stress differentials. a–relationship between fracture count and time steps. b–breakdown pressure and fracture extension radius.

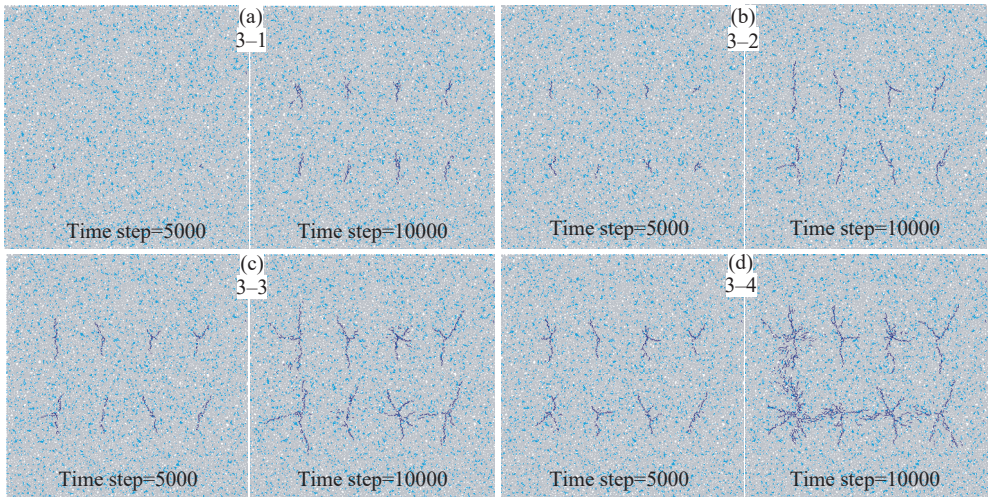

Fig. 9. Fracture distribution after reservoir fracturing under different injection pressure. a–injection pressure 5 MPa. b–injection pressure 10 MPa. c–injection pressure 15 MPa. d–injection pressure 20 MPa.

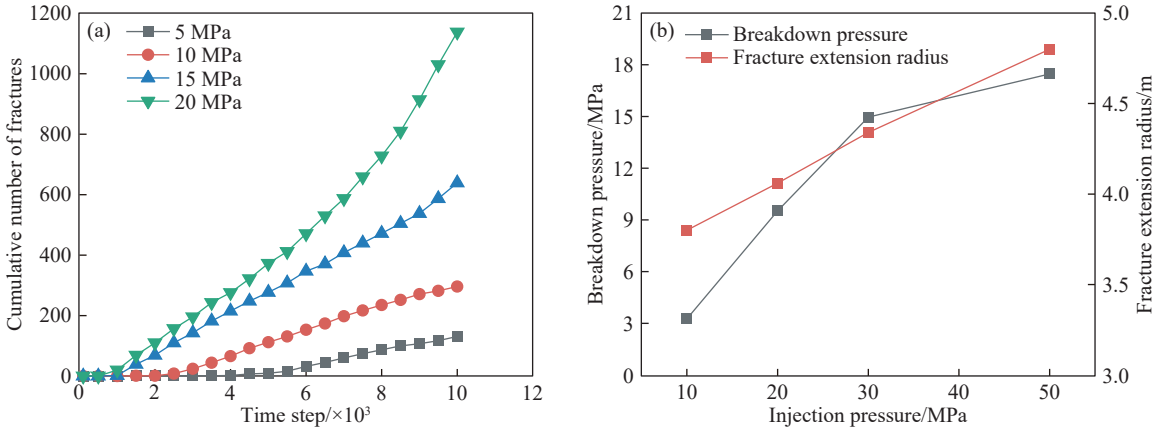

Fig. 10. Reservoir fracture pressure and fracture propagation trends under different injection pressures. a–relationship between fracture count and time steps. b–breakdown pressure and fracture extension radius.

injection points and connect.

Fig. 10 shows the relationship between fractures and time steps in hydrate reservoirs, as well as the variation of hydrate reservoir breakdown pressure and fracture extension radius with fluid injection pressure. Higher injection pressures lead to rapid fracture formation in the early stages of fracturing, with a rapid increase in the number of fractures over time (Fig. 10a). As the injection pressure rises, both the number of fractures and their extension radii increase significantly (Fig. 10b). Moreover, the increased intra-fracture pressure exerts a greater force on the reservoir, thereby extending the fracture distance. At the same time, increased intra-fracture

fluid pressure is more likely to induce hydrate reservoir damage in multiple directions and increase the number of fractures.

3.4. Effect of injection point spacing and horizontal well spacing on fracture extension

Fig. 11 and Fig. 12 show the distribution of fractures and post-fracturing stresses as a function of injection point and horizontal well spacing. An injection point spacing of 6 m and a horizontal well spacing of 8 m result in extensive areas of elevated stress between the points. As a result, fractures deviate from the maximum horizontal principal stress direction, forming multiple main fractures. During this phase, inter-well fracture interference phenomena are more pronounced. Increased spacing between injection points and horizontal wells further weakens the areas of high stress between wells, leading to fractures extending predominantly in the maximum horizontal principal stress direction with a few branching fractures. Further increases in both injection point and horizontal well spacing lessen the effect of inter-fracture stress perturbation, decrease the number of main fractures, and form a small number of branching fractures near the injection points. Near the model boundaries, fractures show turning and bifurcation because of in-situ stresses, while central fractures expand predominantly along the maximum horizontal principal stress direction.

Hydrate reservoir breakdown pressure is negatively correlated with injection point spacing and horizontal well spacing (Fig. 13). This trend is attributed to the fracturing fluid injection rate exceeding the reservoir filtration loss rate, leading to compaction of the reservoir near the injection points and increasing its mechanical strength. By increasing the distance between injection points and horizontal

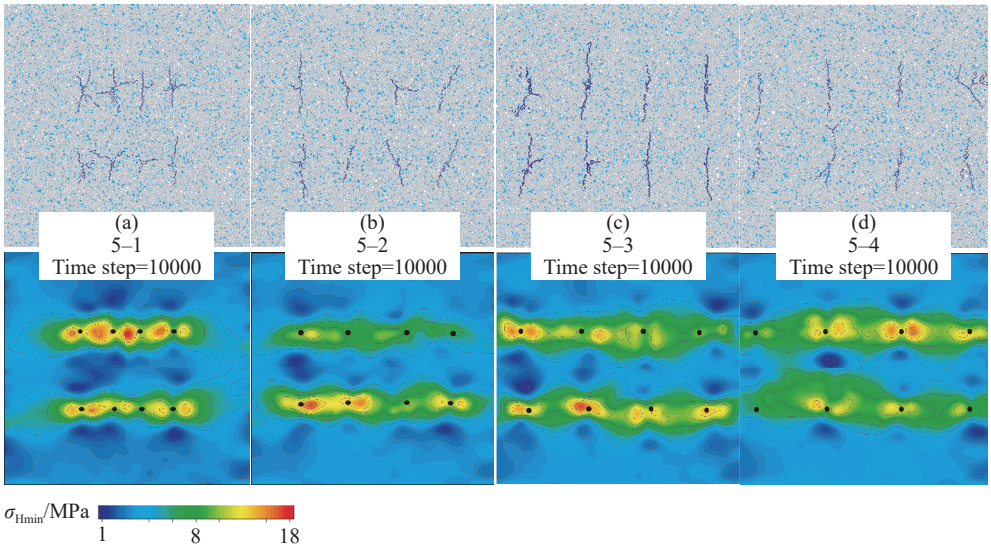

Fig. 11. Fracture distribution and stress cloud after model fracturing with different injection point spacing. a–injection point spacing 6 m. b–injection point spacing 10 m. c–injection point spacing 14 m. d–injection point spacing 18 m.

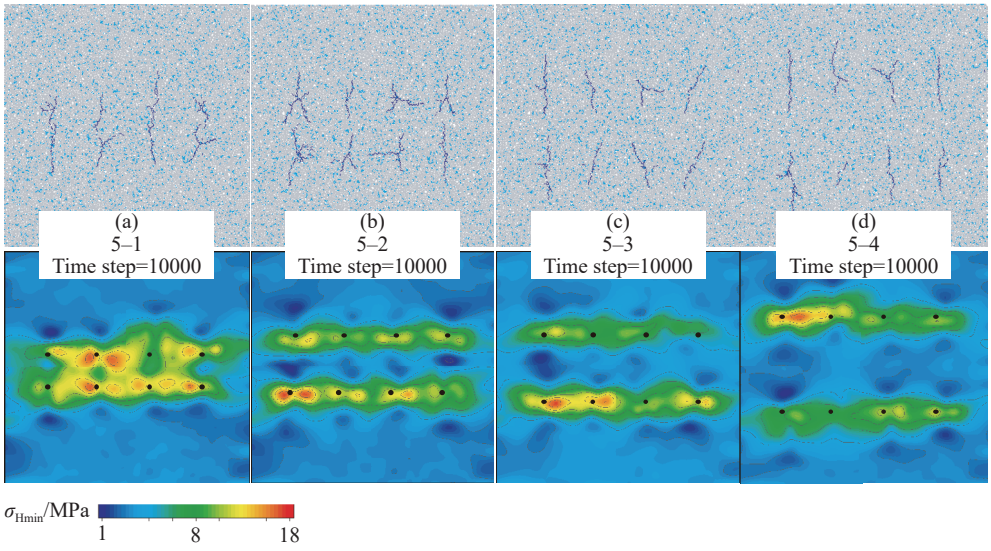

Fig. 12. Fracture distribution and stress cloud after model fracturing with different horizontal well spacing. a–horizontal well spacing 5 m. b-horizontal well spacing 12 m. c–horizontal well spacing 16 m. d–injection point spacing 20 m.

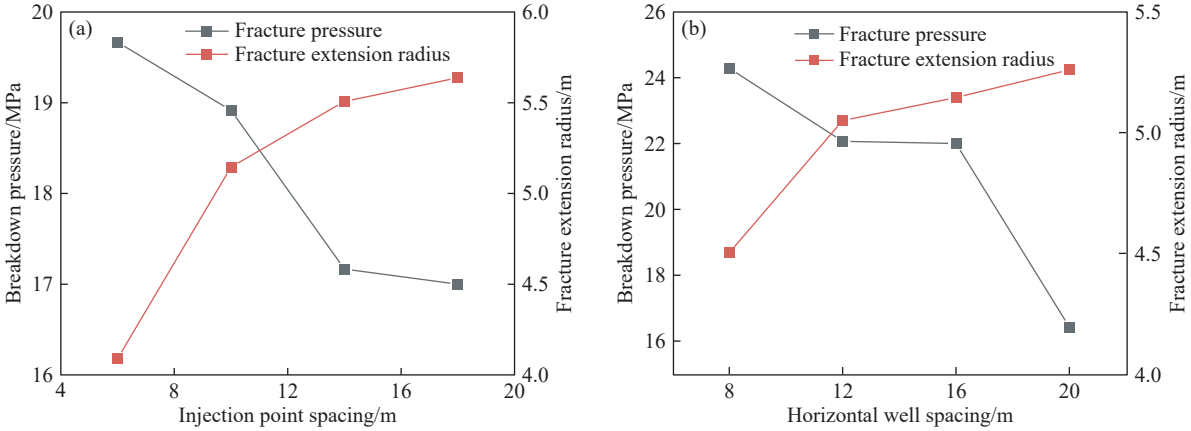

Fig. 13. Breakdown pressure and fracture extension radius in reservoirs under different perforation spacing and horizontal well spacing conditions. a–different injection point spacing. b–different horizontal well spacing.

wellbores, mutual interference among fractures near adjacent injection points is reduced, as well as the stress perturbations induced by water injection. As a result, fractures appear as bi-wing fractures with a corresponding increase in both their number and extension radius.

4. Discussion

4.1. Analysis of the effects of various factors on fracture propagation

Numerical simulations reveal the multiple influences of different factors on fracture initiation and propagation. The pore network model shows hydrate formation within sediment pore spaces changes the size, shape, and connectivity, thus affecting the reservoir porosity and permeability (Blunt MJ et al., 2002). As hydrate saturation increases, more pores are filled, leading to reduced porosity and permeability. At the same time, hydrates increase the elastic modulus and cohesion of the reservoir (Ye JL et al., 2020), raising breakdown pressure and making fracture initiation and propagation more difficult. Changes in the horizontal stress difference affect the direction of fluid seepage of the fluid. Under low horizontal stress difference, multidirectional seepage leads to broader fluid diffusion, compressing the reservoir near the injection point and increasing mechanical strength and fracture pressure. When the horizontal stress difference aligns the fluid seepage in the direction of the maximum principal stress, the well pressure peaks rapidly, triggering reservoir fracturing. This rupture process significantly influences the initiation, propagation, and ultimate failure mode of fractures.

Hydrate saturation and horizontal stress differences influence fracture initiation and propagation by altering the basic physical properties and geological conditions of the reservoir. Injection pressure, injection point spacing, and horizontal well spacing affect fracture initiation and propagation by altering the reservoirs stress distribution. Low injection pressure has a minimal impact on the final damage pattern of the hydrate reservoir. However, high injection pressures result in fracturing fluid discharge at a rate exceeding seepage, thereby modifying the stress field around the injection point. This leads to hydrate reservoir compaction and elevated fracture pressure. Reduced injection point and horizontal wellbore spacing cause more pronounced changes in the hydrate reservoir stress state, leading to extensive areas of contiguous or overlapping high stress. These changes further increase fracture pressure, alter fracture propagation paths and hydrate reservoir failure modes, and significantly increase inter-fracture and horizontal wells interference phenomena.

4.2. Fracture distribution uniformity index

Statistical analysis of the quantity and spatial distribution of fractures is crucial for evaluating the efficacy of hydraulic fracturing operations (Duan K et al., 2021). The concentration or dispersion of the fracture distribution plays a key role in determining the hydrate recovery ratio. This research employed the distribution uniformity index (DUI) proposed by Peng PH et al. (2017) to quantitatively assess the effect of various factors on fracturing effectiveness. The stratigraphic interval was segmented into $2^n \times 2^n$ squares. The number of squares containing fractures, denoted as g(n), and the DUI is defined as the ratio of g(n) to the total number of squares (Eq. 6). A DUI of 0, indicating highly concentrated fractures and sparse distribution elsewhere, reflects poor fracturing results, whereas a DUI of 1, with fractures in every square, indicates ideal fracturing effects.

$$f(n) = \frac{g(n)}{4^n}, n = 0, 1, 2, \ldots \tag{6}$$

Fig. 14 shows the effect of different factors on the DUI. As hydrate saturation increases, the number of post-fracturing fractures decreases with the DUI increases. This indicates that a higher number of fractures does not equate to better hydraulic fracturing results at lower saturations. The reason is that the fractures are mainly concentrated near the injection point, leading to less effective hydraulic fracturing. Increasing hydrate saturation increases the fracture extension radius, thereby increasing the DUI (Fig. 14a). As shown in Fig. 14b, there is no clear linear relationship between horizontal stress

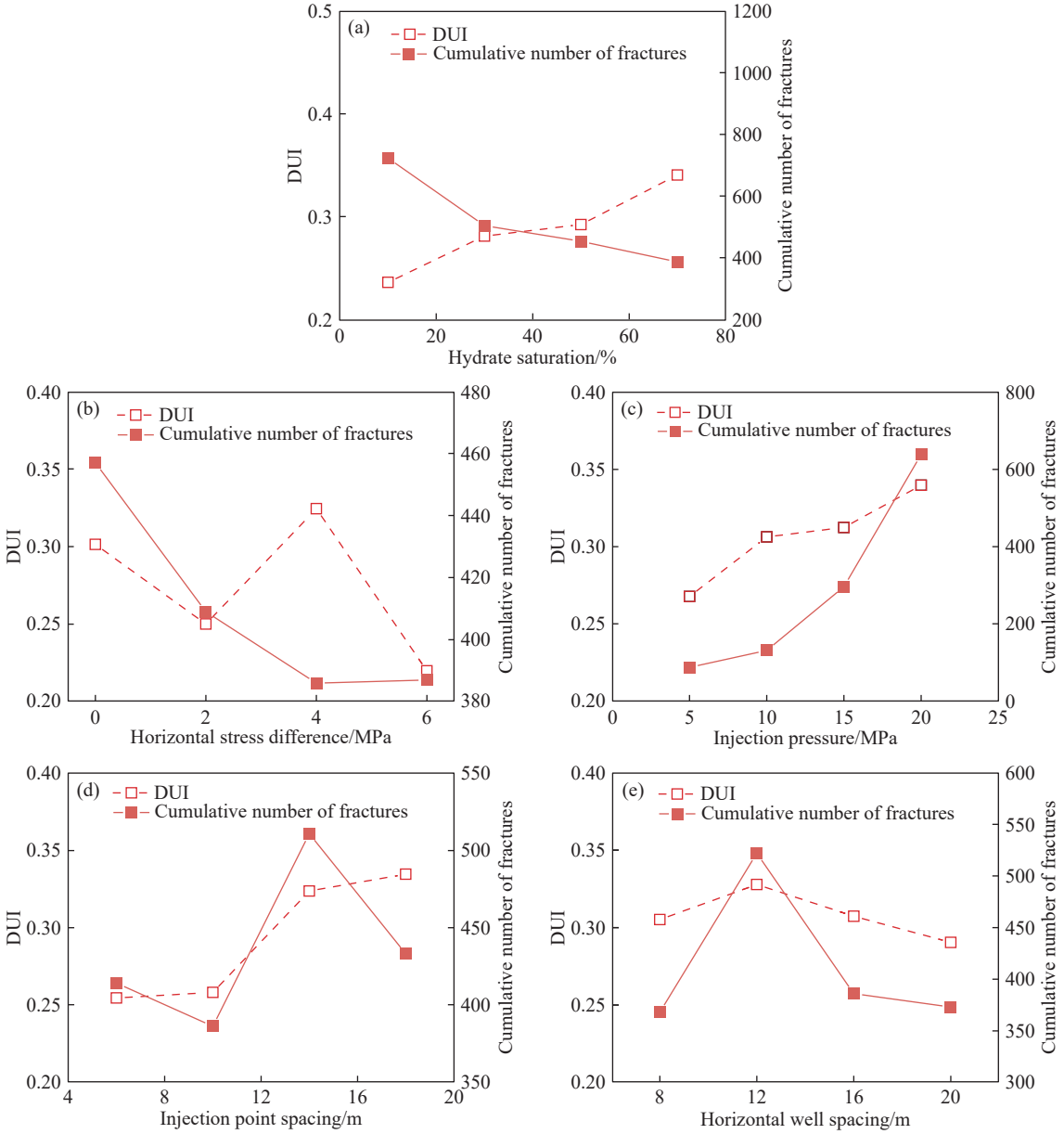

Fig. 14. DUI after reservoir fracturing under the influence of different factors. a–different hydrate saturation. b–different horizontal stress differences. c–different injection pressures. d–different injection point spacing. e–different horizontal well spacing.

differential and DUI. When the horizontal stress differential is small, multiple main fractures appear around the injection point. However, when the horizontal stress differential is large, the number of main fractures decreases while their extension distance increases, resulting in irregular variations in the DUI index. The DUI increase with increasing injection pressure suggesting that higher pressures increase hydrate reservoir damage, spread fractures more widely, and enhance the effectiveness of hydraulic fracturing. When injection point spacing under 10 m, increasing spacing does not result in a higher DUI (Fig. 14c). When injection points spacing exceeds 10 m, the DUI begins to increase with spacing (Fig. 14d) because of stress disturbances between injection point. Closer well spacing often results in interconnected fractures, leading to well interference and uneven fracture distribution. In contrast, increasing horizontal well spacing beyond 12 m leads to a reduction in DUI (Fig. 14e). This decrease results from less high stress areas between wells, causing fracture bifurcation and steering, which enhances fracturing efficiency. Larger horizontal well spacing reduces stress intensity within the inter-well areas, resulting in fewer occurrences of fracture deflection and branching, and subsequently decreasing the uniformity of fracture distribution.

4.3. Implications

In summary, the presence of hydrates increases the complexity of fracture initiation and propagation in hydrate reservoirs. This complexity poses a significant challenge to the development of effective fracturing strategies for these reservoirs. In practical engineering, higher injection pressures and hydrate saturations do not always lead to better fracturing

results. High hydrate saturation increases hydrate reservoir brittleness and facilitates fracture initiation, but also increases the risk of brittle damage to the reservoir and wellbore instability. Increased injection pressure can exacerbate these problems, making fracture area control difficult and potentially leading to serious incidents such as submarine slides. Additionally, hydrates may undergo secondary formation, reducing permeability (Zhang Z et al., 2020). Conversely, low hydrate saturation in reservoirs can lead to sand production and wellbore plugging during fracturing. To mitigate these risks, proppants are used, or other production methods are integrated to ensure safety and optimum recovery. Additionally, fracturing under low-stress differential conditions creates complex, albeit smaller-scale fracture networks. In contrast, high-stress differential conditions typically result in simpler, larger-scale fracture networks. Therefore, it's important to adjust the well completion method based on variations in hydrate saturation within the reservoir to balance the complexity and size of the fracture network.

The analysis of the DUI for different injection points and horizontal well spacing scenarios, along with stress distribution characteristics, shows an increased risk of fracture interference with smaller horizontal well spacing. Increasing both the injection point and horizontal well spacing can mitigate the adverse effects of inter-well fracture interference on operations. Numerical simulations of artificial fracture dimensions, spatial relationships, and stress perturbations between horizontal wells can provide guidance for optimizing well spacing to avoid extensive interference. It’s important to understand that although inter-well interference can negative impact hydraulic fracturing efficiency, it can also positively affect the overall recovery ratio of horizontal wells. Optimizing well spacing for horizontal wells requires balancing the prevention of adverse cross-well interference with leveraging its benefits to enhance hydrate recovery factors. As a result, it's essential to continuously adapt fracturing parameters to the specific geological conditions and reservoir properties, aiming for cost reduction and improved efficiency in hydrate reservoir fracturing.

4.4. Limitations

This study uses a 2D model to address the visualization challenges and high computational demands associated with 3D models. The coupled fluid-solid model simplifies fluid flow assumptions but effectively captures fluid dynamics in sediments, and has been successfully used in hydraulic fracturing studies (Yao YX et al., 2021; Zhao XP et al., 2011). In research on complex issues, 2D models are effective for the initial investigation and validation of 3D problems. They assume a uniform stress state perpendicular to the model plane, allowing simulation of well and perforation spacing impacts horizontally. Although 2D models cannot represent vertical fracture extension, they provide valuable insights into horizontal fracture trends and interactions, essential for understanding fracture propagation laws and well spacing influence, which have been shown to be effective in previous studies (Duan K et al., 2021). However, 2D models cannot fully capture vertical crack propagation and 3D interactions, which may affect prediction accuracy. Further research using 3D model is needed in subsequent studies.

5. Conclusions

A numerical model for hydraulic fracturing in hydrate reservoirs was established using fluid-solid-coupling DEM in this study. The study investigated the effects of hydrate saturation, along with various geological and engineering factors, on fracture propagation around the wellbore and evaluated the fracturing efficacy using the quantitative evaluation methodology (DUI). The main conclusions are succinctly summarized as follows.

(i) Breakdown pressure for hydrate reservoirs exhibits a positive correlation with hydrate saturation. At saturations below 30%, achieving effective fracturing in hydrate reservoirs is difficult and requires a combination of other production enhancement methods. In such cases, techniques such as the use of proppants can be used to improve the stability of hydrate reservoirs. When the hydrate saturation is greater than 30%, hydrate reservoirs can achieve ideal fracturing results and form more main fractures. When dealing with high hydrate saturation, optimizing the fracturing fluid formulation, such as using low-density and low-viscosity fracturing fluids, can further enhance fracturing efficiency.

(ii) A higher horizontal stress difference reduces the number of branching fractures and promotes fracture propagation in the direction of maximum horizontal principal stress. During fracturing operations, reducing injection pressure can increase the extension radius of fractures and can be combined with segmental fracturing to reduce stress interference. Concurrently, the extension radius of fractures increases as the fracturing pressure of the reservoir decreases. Furthermore, a greater horizontal stress difference reduces the stress disturbance between adjacent injection points. It is advisable to adjust fracturing parameters in real-time to maintain the desired fracture extension and complexity.

(iii) The scale of fracturing in hydrate reservoirs expands with increasing injection pressure, while the time required to fracture the reservoir decreases. Extension radius of fractures is positively correlated with injection point spacing and well spacing. The effects of inter-well interference and stress perturbation diminish with increased injection point spacing and well spacing. During hydraulic fracturing, appropriately increase injection pressure to expand fracturing scale, but keep it within the reservoir's fracture tolerance. Designing injection point and well spacing is critical for increasing the crack extension radius, reduce inter-well interference, and utilize positive inter-well interference to ensure fracturing efficiency and construction safety.

CRediT authorship contribution statement

Jia-Wei Zhang, Chang-Ling Liu and Yong-Chao Zhang

conceived of the presented idea. Jia-Wei Zhang and Yong-Chao Zhang carried out the experiment. All authors discussed the results and contributed to the final manuscript.

Declaration of competing interest

The authors declare no conflicts of interest.

Acknowledgements

This study was financially supported by the National Key Research and Development Plan (2023YFC2811001), the National Natural Science Foundation of China (42206233), and the Taishan Scholars Program (tsqn202312280, tsqn202306297). All financial supports are greatly appreciated.

References

Blunt MJ, Jackson MD, Piri M, Valvatne PH. 2002. Detailed physics, predictive capabilities and macroscopic consequences for pore-network models of multiphase flow. Advances in Water Resources, 25, 1069–1089. doi: 10.1016/s0309-1708(02)00049-0.

Chen C, Yang L, Jia R, Sun YH, Guo W. 2000. Simulation study on the effect of fracturing technology on the production efficiency of natural gas hydrate. Energies, 10(8), 1241. doi: 10.3390/en10081241.

Chen XJ, Lu HL, Gu LJ, Shang SL, Zhang Y, Huang X, Zhang L. 2022. Preliminary evaluation of the economic potential of the technologies for gas hydrate exploitation. Energy, 243, 123007. doi: 10.1016/j.energy.2021.123007.

Chen MT, Li YL, Zhang YJ, Qi MH, Wu NW. 2023a. Recent advances in creep behaviors characterization for hydrate-bearing sediment. Renewable and Sustainable Energy Reviews, 183, 113434. doi: 10.1016/j.rser.2023.113434.

Chen MT, Li YL, Zhang PH, Yu GG, Zhang Z, Zhang YJ, Wu NY. 2023b. Numerical simulation of failure properties of interbedded hydrate-bearing sediment and their implications on field exploitation. Ocean Engineering, 274, 114030. doi: 10.1016/j.oceaneng.2023.114030.

Deng SC, Li HB, Ma GW, Huang H, Li X. 2014. Simulation of shale–proppant interaction in hydraulic fracturing by the discrete element method. International Journal of Rock Mechanics and Mining Sciences, 70, 219–228. doi: 10.1016/j.ijrmms.2014.04.011.

Duan K, Li YC, Yang WD. 2021. Discrete element method simulation of the growth and efficiency of multiple hydraulic fractures simultaneously-induced from two horizontal wells. Geomechanics and Geophysics for Geo-Energy and Geo-Resources, 7, 1–20. doi: 10.1007/s40948-020-00196-4.

Ding YL, Qian AN, Lu HL. 2022. Influences of hydrate morphology and hydrate distribution heterogeneity on the mechanical properties of hydrate-bearing sediments using the discrete element method. Geomechanics and Geophysics for Geo-Energy and Geo-Resources, 8(3), 106. doi: 10.1007/s40948-022-00410-5.

Dong L, Liu XQ, Gong B, Li YL. 2024. Geomechanical properties of hydrate-bearing strata and their applications. Advances in Geo-Energy Research, 11(3), 161–167. doi: 10.46690/ager.2024.03.01.

Feng YC, Chen L, Suzuki A, Kogawa T, Okajima J, Komiya A, Maruyama S. 2019. Enhancement of gas production from methane hydrate reservoirs by the combination of hydraulic fracturing and depressurization method. Energy Conversion and Management, 184(1), 194–204. doi: 10.1016/j.enconman.2019.01.050.

Gu XQ, Huang MS, Qian JG. 2014. DEM investigation on the evolution of microstructure in granular soils under shearing. Granular Matter, 16(1), 91–106. doi: 10.1007/s10035-013-0467-z.

Hyodo M, Wu Y, Nakashima K, Kajiyama S, Nakata Y. 2017. Influence of fines content on the mechanical behavior of methane hydrate-bearing sediments. Journal of Geophysical Research. Solid Earth, 122(10), 7511–7524. doi: 10.1002/2017jb014154.

Ishida MT. 2011. The distinct element analysis for hydraulic fracturing in hard rock considering fluid viscosity and particle size distribution. International Journal of Rock Mechanics and Mining Sciences, 48(5), 712–727. doi: 10.1016/j.ijrmms.2011.04.013.

Jung JW, Santamarina JC. 2011. Hydrate adhesive and tensile strengths. Geochemistry, Geophysics, Geosystems, 12(8), Q08003–Q08011. doi: 10.1029/2010gc003495.

Konno Y, Jin Y, Yoneda J, Uchiumi T, Shinjou K, Nagao J. 2016. Hydraulic fracturing in methane-hydrate-bearing sand. RSC Advances, 6(77), 73148–73155. doi: 10.1039/c6ra15520k.

Lei Q, Xu Y, Cai B, Guan BS, Wang X, Bi GQ, Li H, Li S, Ding B, Fu HF, Tong Z, Li T, Zhang H. 2022. Progress and prospects of horizontal well fracturing technology for shale oil and gas reservoirs. Petroleum Exploration and Development, 49(1), 191–199. doi: 10.1016/s1876-3804(22)60015-6.

Li FG, Yuan Q, Li TD, Li Z, Sun CY, Chen GJ. 2019. A review: enhanced recovery of natural gas hydrate reservoirs. Chinese Journal of Chemical Engineering, 27(9), 2062–2073. doi: 10.1016/j.cjche.2018.11.007.

Li JF, Ye JL, Qin XW, Qiu HJ, Wu NY, Lu HL, Xie WW, Lu JA, Peng F, Xu ZQ, Lu C, Kuang ZG, Wei JQ, Liang QY, Lu HF, Kou BB. 2018. The first offshore natural gas hydrate production test in South China Sea. China Geology, 1(1), 5–16. doi: 10.31035/cg2018003.

Li YH, Wu P, Sun X, Liu WG, Song YC. 2021. Mechanical behaviors of hydrate-bearing sediment with different cementation spatial distributions at microscales. iScience, 24(5), 102448. doi: 10.1016/j.isci.2021.102448.

Li ZF, Chow JK, Li JH, Tai P, Zhou ZS. 2022. Modeling of flexible membrane boundary using discrete element method for drained/undrained triaxial test. Computers and Geotechnics, 145, 104687. doi: 10.1016/j.compgeo.2022.104687.

Li B, Shen YF, Sun YF, Qi Y, Shan HF, Zhang GB. 2024a. Assessing hydraulic fracturing feasibility in marine hydrate reservoirs: Impact of closure pressure and hydrate decomposition on fracture conductivity. Ocean Engineering, 309, 118569. doi: 10.1016/j.oceaneng.2024.118569.

Li XY, Wang Y, Li XS, Zhou SD, Liu Y, Lv XF. 2024b. Study on the production of gas hydrates and underlying free gas by horizontal well under different directions of hydraulic fracturing. Energy, 290, 130199. doi: 10.1016/j.energy.2023.130199.

Liao SZ, Hu JH, Zhang Y. 2022. Investigation on the influence of multiple fracture interference on hydraulic fracture propagation in tight reservoirs. Journal of Petroleum Science and Engineering, 211, 110160. doi: 10.1016/j.petrol.2022.110160.

Liu XQ, Zhang WD, Qu ZQ, Guo TK, Sun Y, Rabiei M, Cao QY. 2020. Feasibility evaluation of hydraulic fracturing in hydrate-bearing sediments based on analytic hierarchy process-entropy method (AHP–EM). Gas Science and Engineering, 81, 103434. doi: 10.1016/j.jngse.2020.103434.

Liu Y, Li G, Chen J, Bai Y, Hou J, Xu H, Zhao E, Chen Z, He J, Zhang L. 2023. Numerical simulation of hydraulic fracturing-assisted depressurization development in hydrate bearing layers based on discrete fracture models. Energy, 263, 126146. doi: 10.1016/j.energy.2022.126146.

Liu H, Lu HL, Zhang KN. 2023. Embedded discrete fracture model for investigating the effect of fractures on gas hydrate production. Energy and Fuels, 37(20), 15768–15783. doi: 10.1021/acs.energyfuels.3c02819.

Ma KL, Li DL, Liang DQ. 2023. Reservoir stimulation technologies for natural gas hydrate: research progress, challenges, and perspectives. Energy and Fuels, 37(4), 10112–10133. doi: 10.1021/acs.energyfuels.3c01464.

Peng PH, Ju Y, Wang YL, Wang SQ, Gao F. 2017. Numerical analysis of the effect of natural microcracks on the supercritical CO2 fracturing crack network of shale rock based on bonded particle models. International Journal for Numerical and Analytical Methods in Geomechanics, 41(18), 1992–2013. doi: 10.1002/nag.2712.

Ruppel CD, Kessler JD. 2017. The interaction of climate change and methane hydrates. Reviews of Geophysics, 55(1), 126–168. doi: 10.1002/2016rg000534.

Su PB, Wei W, Sun YB, Lü YY, Cheng H, Han WF, Zhang W, Liang JQ. 2024. Geological reservoir and resource potential ($10^{13}m^3$) of gas hydrates in the South China Sea. China Geology, 7(3), 422–444. doi: 10.31035/cg2024069.

Shaibu R, Sambo C, Guo B, Dudun A. 2021. An assessment of methane gas production from natural gas hydrates: Challenges, technology and market outlook. Advances in Geo-Energy Research, 5(3), 318–332. doi: 10.46690/ager.2021.03.07.

Sun CY, Li WZ, Yang X, Li FG, Yuan Q, Mu L, Chen J, Liu B, Chen GJ. 2011. Progress in Research of Gas Hydrate. Chinese journal of chemical Engineering, 19(1), 151–162. doi: 10.1016/S1004-9541(09)60192-0.

Sun JX, Ning FL, Liu TL, Liu CL, Chen Q, Li YL, Cao XX, Mao PX, Zhang L, Jiang GS. 2019. Gas production from a silty hydrate reservoir in the South China Sea using hydraulic fracturing: A numerical simulation. Energy Science and Engineering, 7(4), 1106–1122. doi: 10.1002/ese3.353.

Tavarez FA, Plesha ME. 2007. Discrete element method for modelling solid and particulate materials. International Journal for Numerical Methods in Engineering, 70(4), 379–404. doi: 10.1002/nme.1881.

Too JL, Cheng A, Khoo BC, Palmer A, Linga P. 2018. Hydraulic fracturing in a penny-shaped crack. Part II: Testing the frackability of methane hydrate-bearing sand. Gas Science and Engineering, 52, 619–628. doi: 10.1016/j.jngse.2018.01.046.

Wang ZY, Liao YQ, Zhang WD, Sun BJ, Sun XH, Deng XJ. 2018. Coupled temperature field model of gas-hydrate formation for thermal fluid fracturing. Applied Thermal Engineering, 133, 160–169. doi: 10.1016/j.applthermaleng.2018.01.039.

Wu P, Li YH, Sun X, Liu WW, Song Y. 2020. Mechanical characteristics of hydrate-bearing sediment: a review. Energy and Fuels, 35(2), 1041–1057. doi: 10.1021/acs.energyfuels.0c03995.

Wei RC, Liu LL, Jia C, Dong X, Bu QT, Zhang YC, Liu CL, Wu NY. 2023. Undrained triaxial shear tests on hydrate-bearing fine-grained sediments from the shenhu area of south china sea. Journal of Marine Science and Engineering, 11(1604), 1604. doi: 10.3390/jmse11081604.

Xu JC, Qin HT, Li HY, Lu C, Li SX, Wu DD. 2023. Enhanced gas production efficiency of class 1, 2, 3 hydrate reservoirs using hydraulic fracturing technique. Energy, 263, 126003. doi: 10.1016/j.energy.2022.126003.

Yao YX, Guo ZH, Zeng JM, Li DL, Lu JL, Liang DQ, Jiang MJ. 2021. Discrete element analysis of hydraulic fracturing of methane hydrate-bearing sediments. Energy and Fuels, 35(8), 6644–6657. doi: 10.1021/acs.energyfuels.1c00248.

Ye JL, Qin XW, Xie WW, Lu HL, Ma BJ, Qiu HJ, Liang JQ, Lu JA, Kuang ZG, Lu C, Liang QY, Wei SP, Yu YJ, Liu CS, Li B, Shen KX, Shi HX, Lu QP, Li J, Kou BB, Song G, Li B, Zhang HE, Lu HF, Ma C, Dong YF, Bian H. 2020. The second natural gas hydrate production test in the South China Sea. China Geology, 3(2), 197–209. doi: 10.31035/cg2020043.

Yu T, Guan GQ, Wang DY, Song YC, Abudula A. 2021. Gas production enhancement from a multilayered hydrate reservoir in the South China Sea by hydraulic fracturing. Energy and Fuels, 35(15), 12104–12118. doi: 10.1021/acs.energyfuels.1c01785.

Zhao JZ, Ren L, Shen C, Li YM. 2018. Latest research progresses in network fracturing theories and technologies for shale gas reservoirs. Natural Gas Industry B, 5(5), 533–546. doi: 10.1016/j.ngib.2018.03.007.

Zhao XP, Paul YR. 2011. Numerical modeling of seismicity induced by fluid injection in naturally fractured reservoirs. Geophysics, 76(6), WC167–WC180. doi: 10.1190/geo2011-0025.1.

Zhou J, Jin Y, Chen M. 2010. Experimental investigation of hydraulic fracturing in random naturally fractured blocks. International Journal of Rock Mechanics and Mining Sciences, 47(7), 1193–1199. doi: 10.1016/j.ijrmms.2010.07.005.

Zhou J, Zhang LQ, Pan ZJ, Han ZH. 2016. Numerical investigation of fluid-driven near-borehole fracture propagation in laminated reservoir rock using PFC2D. Gas Science and Engineering, 36, 719–733. doi: 10.1016/j.jngse.2016.11.010.

Zhang YC, Liu LL, Hu GW, Bu QT, Li CF, Zhang ZC. 2022. Formation mechanism, experimental method, and property characterization of grain-displacing methane hydrate in marine sediment: A review. China Geology, 5(2), 345–354. doi: 10.31035/cg2022014.

Zhang Z, Li CF, Ning FL, Liu LL, Cai JC, Liu CL, Wu NY, Wang DG. 2020. Pore fractal characteristics of hydrate-bearing sands and implications to the saturated water permeability. Journal of Geophysical Research: Solid Earth, 125(3), e2019JB018721. doi: 10.1029/2019jb018721.

Zhang Z, Liu LL, Lu WJ, Liu CL, Ning FL, Dai S. 2023. Permeability of hydrate-bearing fine-grained sediments: Research status, challenges and perspectives. Earth-Science Reviews, 244, 104517. doi: 10.1016/j.earscirev.2023.104517.